Design Engineering

ISSN: 0011-9342 | Year 2021
Issue: 6 | Pages: 5143-5155

Substantial reduction of NIR electromagnetic reflectance based on rare-earth-doped nanomaterial.

Y. A. Saeid[1,2], Ebtesam E. Ateia[1], Ahmed Fawzy[3], and M.K. Abdelmaksoud[1,4*]

[1]Physics Department, Faculty of Science, Cairo University, Giza, 12613, Egypt.

[2]Physics Department, Higher Institute of Engineering and Technology, New Cairo Academy, Cairo, Egypt.

[3*]Nanotechnology central lab, Electronic Research Institute (ERI),Cairo, 12622, Egypt.

[4]Faculty of Nanotechnology for postgraduate studies, Cairo University, El-Sheikh Zayed, 12588, Egypt.

*Correspondence: mkbedir@gmail.com; Tel.: (+02 01017172531)

Abstract:

A novel nanomaterial for electromagnetic absorption applications was manufactured. The samples are prepared through the citrate auto combustion method by doping Calcium nano ferrite with rare earth elements (samarium and gadolinium) with the specific compositions $CaFe_{2-x-y}Gd_xSm_yO_4$ (x = y = 0.0, x = 0.025, y = 0.05). X-ray diffraction showed that the samples are successfully produced in a single-phase regime, with measured crystallite sizes of 21 and 18 nm. HRTEM showed a uniform distribution of the particles in the samples of hexagonal shape with well-defined boundaries. Elemental analysis is showed by using EDAX. Moreover, UV-VIS-NIR diffuse reflectance spectroscopy is used to prove that the proposed composition improves the performance of electromagnetic absorption. Then, the optical energy gaps of the pristine and doped samples are compared. Meanwhile, the obtained results proposed a promising method based on calcium nano ferrite to prepare a cheap, lightweight, and wideband absorber. The photoluminescence property was studied using 225 nm to 400 nm radiation source with step 25 nm. Furthermore, the suggested composition has great potential in other related applications like solar energy harvesting, biosensing, and photonic detection.

Keywords: Band gap, $CaFe_2O_4$, Nanomaterials, Photoluminescence, Rare earth.

I. INTRODUCTION

Modern devices like wireless sensor equipment, radar systems, and mobile phones require a microwave absorption material [1], [2]. The microwave absorbents are classified according to their mechanism of work, whereas their essential properties are the broad absorption bandwidth and lightweight. To achieve these requirements, a combination of two or more nanomaterials can be used to adjust the parameters of the absorber.

ISSN: 0011-9342 | Year 2021
Issue: 6 | Pages: 5143-5155

For example, the composites like Fe/SiO_2 [3], Fe_3O_4@TiO_2, Fe_3O_4@ZnO_2[4], $MnFe_2O_4$ [5], carbon-based composites and nanocomposites have been extensively studied lately. Generally, there are a variety of applications at various frequency ranges, and one of the most important applications is solar energy harvesting. Specifically, many types of coatings have been used for energy harvesting such as multilayer absorbers, textured low bandgap semiconductors as well as metallic based on nanomaterials composite coatings [6], [7].

Currently, many researchers work to improve efficiency, minimize material consumption, and widen the spectrum for energy harvesting systems[8], [9]. In particular, one main focus is to suppress waves in the infrared region, which is used intensively in military applications. Recently, nanomaterials based on ferrite were used to synthesize electromagnetic absorber because they introduce easy, cheap, free to tailor the emission spectrum and low weight method for fabrication. Calcium ferrites ($CaFe_2O_4$) have been used in this paper due to their important applications, and for their use in high-temperature sensors, absorbers, etc. Besides, it shows significant physical characteristics, such as high thermal stability, which makes it applicable over a wide temperature range. Nanocrystalline $CaFe_2O_4$ material with spinel structure was synthesized by different methods like polymerized complex (PC) method, conventional solid-state reaction (SSR) method, citrate precursor method, and auto combustion method. Auto combustion method is an effective, low-cost method, and energy saving for production of nanomaterials.

In this paper, a novel material of rare-earth-doped Calcium nano ferrite has been introduced through the citrate- nitrate method to obtain a sample that can be utilized as an electromagnetic absorber. This will be verified through structural as well as optical properties investigations.

II. MATERIALS AND METHODOLOGY

$CaFe_2O_4$ belongs to the spinel ferrites family. As a result of its unique optical properties, spinel ferrites have attracted a lot of attention. Normally, the spinel structure has the form (A) [B_2] O_4, which is described as a cubic closed pack of oxygen ions. The optical and chemical properties of spinel ferrites are influenced by the synthesis route since it controls the stoichiometry and morphology of the material.

To achieve a small particle size distribution, nanocrystalline calcium ferrite samples were prepared by using the citrate auto combustion method [10]. In this method, the stoichiometric quantities of $Fe(NO_3)_3.9H_2O$ and $Ca(NO_3)_2.4H_2O$ were dissolved in double distilled water and stirred well using a magnetic stirrer, followed by drying as illustrated in Fig. 1.

III. EXPERIMENTAL WORK

Novel nanomaterials with compositions $CaFe_{2-x-y}Gd_xSm_yO_4$ (x = y = 0.0, x = 0.025, y = 0.05) were synthesized by the citrate auto combustion method. Fig. 2 illustrates the anticipated influence of the rare earth doped $CaFe_2O_4$ on the absorption of infrared radiation. Where figure 2a indicates the infrared ray's transmission as the rays go past $CaFe_2O_4$ sample. After the rare-earth doping, the

ISSN: 0011-9342 | Year 2021
Issue: 6 | Pages: 5143-5155

material acts as a network and absorbs the infrared rays as shown in fig. 2(b,c). Specifically, XRD is used to study the crystallinity of the investigated samples. The XRD is a very important tool to check the phase purity and to find out the average crystallite size, as well as the lattice parameters. The average nanoparticle sizes were estimated using Scherrer's relationship. XRD reveals the variation in the structure and lattice parameters as a result of the doping [11].

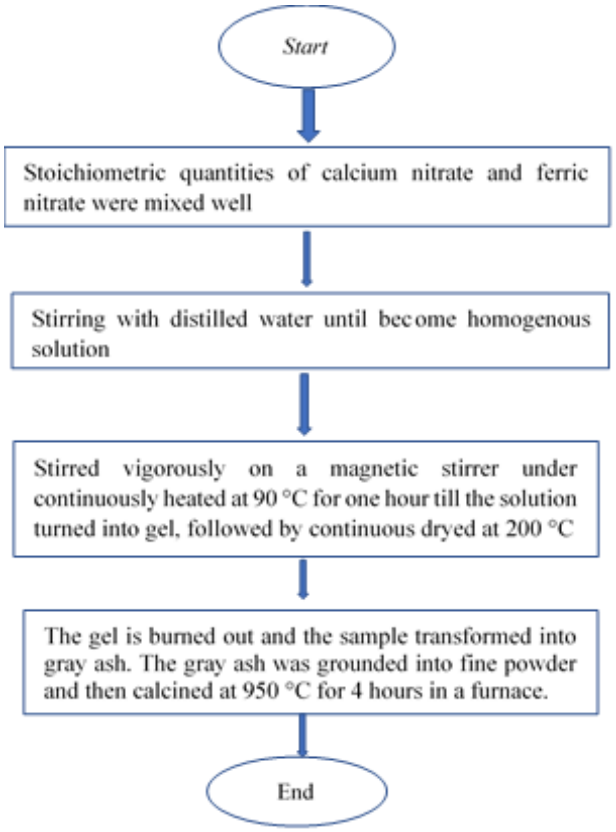

Fig 1: Flowchart describing the preparation method of the samples $CaFe_{2-x-y}Gd_xSm_yO_4$ (x = y = 0.0, x = 0.025, y = 0.05).

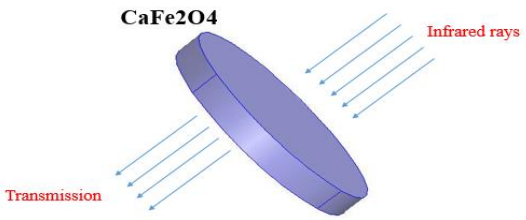

(a)

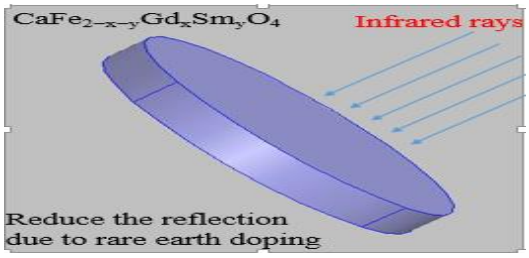

(b)

ISSN: 0011-9342 | Year 2021
Issue: 6 | Pages: 5143-5155

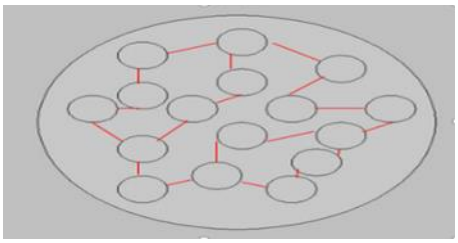

(c)

Fig 2: Schematic illustration of the method of absorption in: (**a)** $CaFe_2O_4$. (**b)** $CaFe_{2-x-y}Gd_xSm_yO_4$ (x = y = 0.0, x = 0.025, y = 0.05). (**c)** Effect of rare earth doping in increasing absorption rate.

Fig. 3 illustrates the XRD pattern for the samples $CaFe_{2-x-y}Gd_xSm_yO_4$ (x = y = 0.0, x = 0.025, y = 0.05). The analysis of the XRD pattern reveals the formation of the structure without contamination. All peaks are well-matched with the standard $CaFe_2O_4$ spectra (ICDD 72-1199). The crystallite size, lattice parameters, theoretical density, and tolerance of the samples are computed based on XRD measurements, as shown in table 1. The tolerance factors are very close to unity which means that the prepared samples have minimal distortion.

The HRTEM micrographs of the solution of the samples are shown in Fig. (4). The micrograph revealed a uniform distribution of the particles of varying shape with well-defined boundaries. The particle shape of the calcium ferrite sample is roughly hexagonal with a little agglomeration, as shown in Fig. 4a. Moreover, the rare-earth-doped calcium ferrite, CaRE, sample shows a relatively higher agglomeration, as presented in Fig. 4b. Generally, the particles display a somewhat homogeneous distribution indicating a proper physical mixing. The particle-size varies in the range of 25 to 65 nm, as can be perceived from Fig. 4.

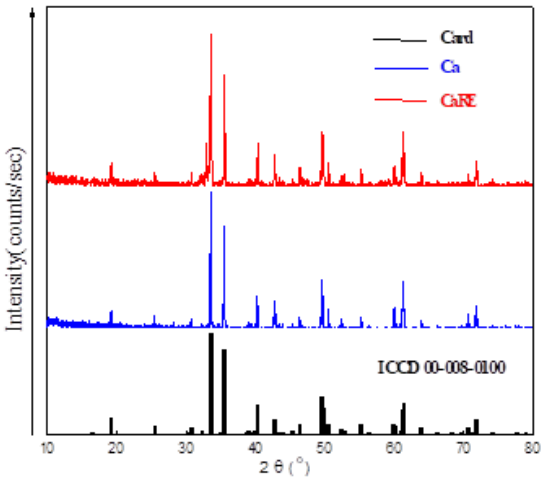

Fig 3: XRD pattern of the samples $CaFe_{2-x-y}Gd_xSm_yO_4$ (x=y= 0.0, x= 0.025, Y=0.05).

Design Engineering

ISSN: 0011-9342 | Year 2021
Issue: 6 | Pages: 5143-5155

TABLE I. Properties of the materials deduced from XRD.

		Ca	CaRE
Crystallite size, D (nm)		21	18
Theoretical density, Dx (gm/cm^3)		4.858	5.022
Lattice parameters	a (nm)	0.945	0.905

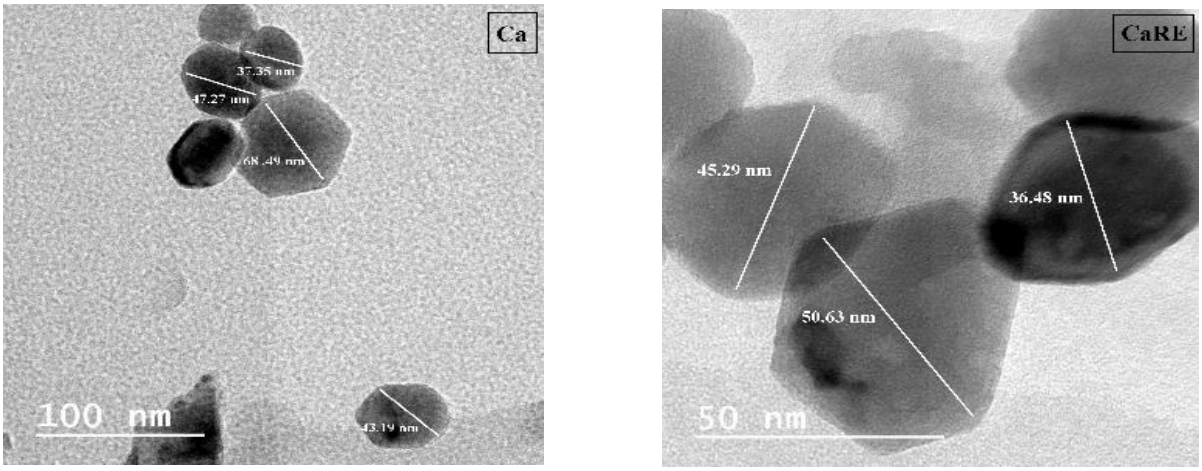

(a) **(b)**

Fig 4: HRTEM micrographs for the samples $CaFe_{(2-x-y)}Gd_xSm_yO_4$ prepared by combustion method: (a) Ca (b) CaRE.

Fig. 5(a) shows the idea of studying the surface microstructure of, the rare-earth-doped calcium ferrite, CaRE, NPs which was done by observing the SEM image. The SEM photograph of sample helps to know the shape of the particles. The nanoparticles have been calcined at 950°C. The results proved that the higher the calcination temperature, the bigger particles were absorbed. In Fig. 5(b), EDX analysis from the spectrum showed that the Fe, Ca, Gd, Sm, and O elements have been found in the sample as the synthesized $CaFe_{2-x-y}Gd_xSm_yO_4$ were formed.

Design Engineering

ISSN: 0011-9342 | Year 2021
Issue: 6 | Pages: 5143-5155

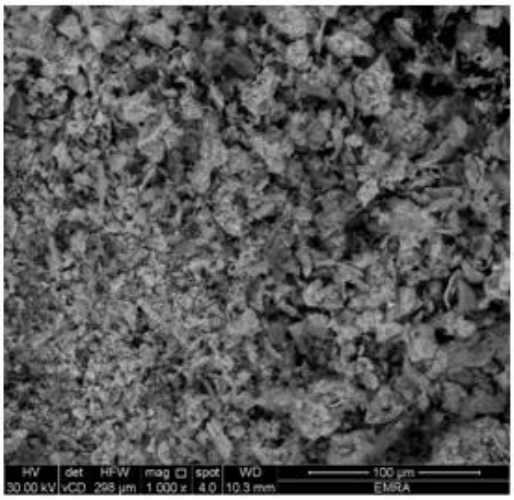

Element	Weight percentage (Wt %)		Atomic percentage (At %)	
	Expected	EDAX analysis	Expected	EDAX analysis
Ca	17.97	16.42	14.29	13.03
Fe	48.21	50.47	27.5	28.81
Gd	1.76	1.79	0.36	0.36
Sm	3.37	4.17	0.71	0.88
O	28.69	27.15	57.14	56.92

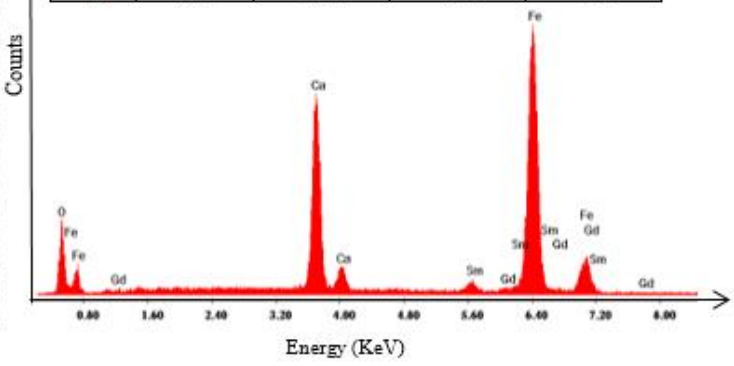

(a) (b)

Fig 5: (a)SEM micrographs, (b) EDX analysis of $CaFe_{2-x-y}Gd_xSm_yO_4$ (x = y = 0.0, x = 0.025, y = 0.05).

IV. RESULTS AND DISCUSSION

4.1 UV-VIS-NIR

The optical properties of the samples pellets were probed using UV-VIS-NIR diffuse reflectance spectroscopy (DRS). DRS spectroscopy is a spectroscopic technique based on the reflection of light in the different-wavelength-regions by a powdered sample[11], [12]. Applying the DRS technique, both d-d and charge transfer transitions of supported transition-metal-ions can be probed, therefore, the technique is useful in exploring heterogeneous catalysts. Moreover, the optical bandgap of the inspected samples is easily evaluated from DRS measurements[13]. Typically, the ratio of the light scattered from a thick-layer-sample and that from an ideal non-absorbing reference sample is measured as a function of the wavelength λ [14]. Explicitly, the diffuse reflectance of the sample ($R\infty$) is related to its absorption (K), and scattering (S) coefficients through the Schuster–Kubelka–Munk (SKM) remission function [15]:

$$F(R_\infty) = \frac{(1-R_\infty)^2}{2R_\infty} = \frac{K}{S} \qquad (1)$$

Therefore, the remission function, $F(R_\infty)$, relates the experimentally determined diffuse reflectance of a relatively thick sample to the absorption and scattering coefficients. Consequently, at a constant scattering coefficient, $F(R_\infty) = K$, and the plot of $F(R_\infty)$ vs. concentration of absorbing species will yield a linear relationship. This relation may be used for quantitative investigations on powder samples with infinite thickness enclosing a uniform distribution of metal ions in low concentration. The remission function also depends strongly on particle size for weak absorbers

ISSN: 0011-9342 | Year 2021
Issue: 6 | Pages: 5143-5155

but not for strong absorbers, which absorb almost all the incident photons [13]. Fig. (6) shows the DRS spectra of the investigated samples, where several reflection bands appeared within the different electromagnetic regions. The NIR portion covers the overtones and combination bands of the fundamental stretching frequencies of surface molecular groups such as H2O, O–H, and CO_2. These bands are larger in intensity and excellently measured in diffuse reflectance rather than in transmission mode because of the large scattering involved in the NIR region. Doping $CaFe_2O_4$ with tiny amounts of rare earth elements.

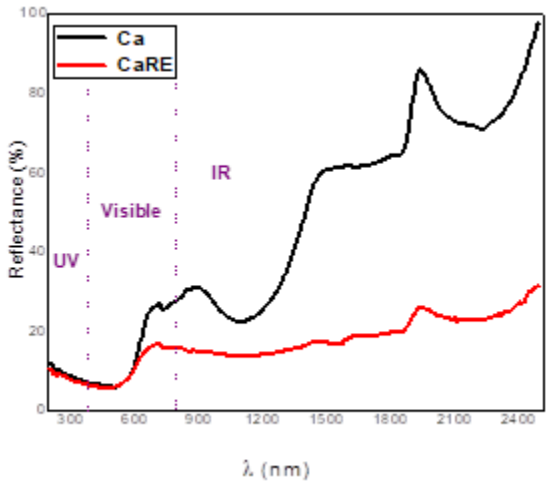

Fig 6: UV-Vis-NIR-diffuse reflectance spectra for the inspected samples.

According to the Kubelka-Munk theory, the Schuster–Kubelka–Munk function is given in terms of the optical bandgap (Eg) as:

$$F(R_\infty) = A(h\nu - E_g)^n \quad (2)$$

Where h is Planck's constant, ν is the frequency of vibration, and A is a proportionality constant. The value of the exponent n signifies the nature of the transition, with n = ½ or 2 for the direct/indirect allowed transition, respectively. Therefore, the bandgap energy may be evaluated from the reflectance spectra by extrapolating the straight-line plot of $(F(R\infty)*h\nu)^2$ or $(F(R\infty)*h\nu)^{1/2}$ versus (hν) as shown in Fig. (7:a-b) [16], [17]. Eg is the intercept of the straight line with the hν-axis when the plotted function on the y-axis vanishes.

The obtained optical, allowed-direct, band gap values are almost the same and equal about 2.0 eV. Consequently, the rare earth doping does not change the direct bandgap value. On the other hand, the band gaps for the allowed-indirect transition are 1.6 and 0.9 eV for the parent and doped samples, respectively. Meanwhile, The bandgap energy of a material is related to its photocatalytic activity of the degradation of pollutants[18]–[20]. Since, the well-known wavelength-energy relation is formulated as, λ = 1240 (eV.nm)/E (eV). Therefore, to overcome the energy gap of 2.0 eV, a photon with a wavelength of 620 nm is required. Namely, to generate electron-hole pairs,

ISSN: 0011-9342 | Year 2021
Issue: 6 | Pages: 5143-5155

which are the dynamic ingredients for the degradation mechanism, we need photons in the visible light regime. This manifests the significance of these samples as excellent photocatalysis-candidates. Hence, the investigated samples are recommended to be used in the photodegradation of pollutants with the application of just visible light.

TABLE II: Allowed direct and indirect Optical energy band values.

Transition / Sample	ALLOWED-DIRECT/ eV	ALLOWED-INDIRECT/ eV
CA	2.0	1.6
CARE	2.0	0.9

4.2 Photoluminescence (PL)

Photoluminescence is considered as a very important phenomenon as in which the emission of light occurs from the material under optical excitation. When a light with sufficient energy falls on a material, photons are absorbed causing electronic excitations [21]. After that, these excitations relax, and the electrons go back to the ground state. When the radiative relaxation occurs, it causes the photoluminescence to take place as shown in figure 8. Since the excitation wavelength may effect on the photoluminescence of any material, the absorption of a material depends strongly on the energy of the incident light. According to that, the selection of the excitation light is considered a very critical part in any photoluminescence study of material. The density of photo-excited electrons and holes has been controlled by the excitation wavelength and this also controls the behavior of these carriers. In this paper, the photoluminescence spectrum of the $CaFe_2O_4$ NPs has been studied using Spectrometer with 225 nm, 250 nm, 275 nm, 300 nm, 325 nm, 350 nm, 375 nm, and 400 nm radiation source. The PL measured for Ca and CaRE to show the effect of rare earth materials on the optical properties of calcium ferrites. The spectrum consists of emission peaks at 605 nm (2.04 eV), 608 nm (2.039 eV) for Ca and CaRE respectively as shown in Fig. 9. On the other hand, the emission intensity of the peaks is strongly dependent upon the excitation wavelength. Furthermore, the quantum confinement may explain the mechanism of PL. Moreover, the shortening of the super-exchange interaction bond length in the nano-crystalline ferrites may be described by this confinement. Which in turn, leads to modification of the electronic structure of ferrite. Alternatively, PL may be explained by the presence of the fast non-radiative relaxation channels which are taking place at the surface of the nanocrystals[22], [23]. The emission spectra have been found in the wavelength range from 560 to 640 nm. From Fig. 9, the band gap energy Eg of the sample may be estimated from the UV emission. Where the UV emission broadband can be attributed to band-to-band transition. A photoluminescence spectra indicate the separation and

ISSN: 0011-9342 | Year 2021
Issue: 6 | Pages: 5143-5155

recombination of photogenerated carriers in the photocatalytic processes[24][25]. Therefore, the PL investigations could quantify the interfacial charge transfer dynamics between the individual components of the examined sample. The pure $CaFe_2O_4$ and the RE-doped sample display emission bands centered at 604 nm, and 608 nm, respectively. Hence, the center of the emission band changes only slightly as a result of the RE doping. Consequently, the Eg value is estimated from the PL spectra to be about 2.05 eV, with the RE-doping making no appreciable difference in the energy gap value. Moreover, the obtained Eg result agrees very well with the energy gap determined from the allowed direct transition using Tauc plots. For the two explored samples, as the excitation wavelength gets longer (lower energy) the intensity of the emitted spectrum decline, as expected. However, for the pure ferrite sample, the emission band width varies from 587 to 620 nm for the excited wavelength of 225 nm.

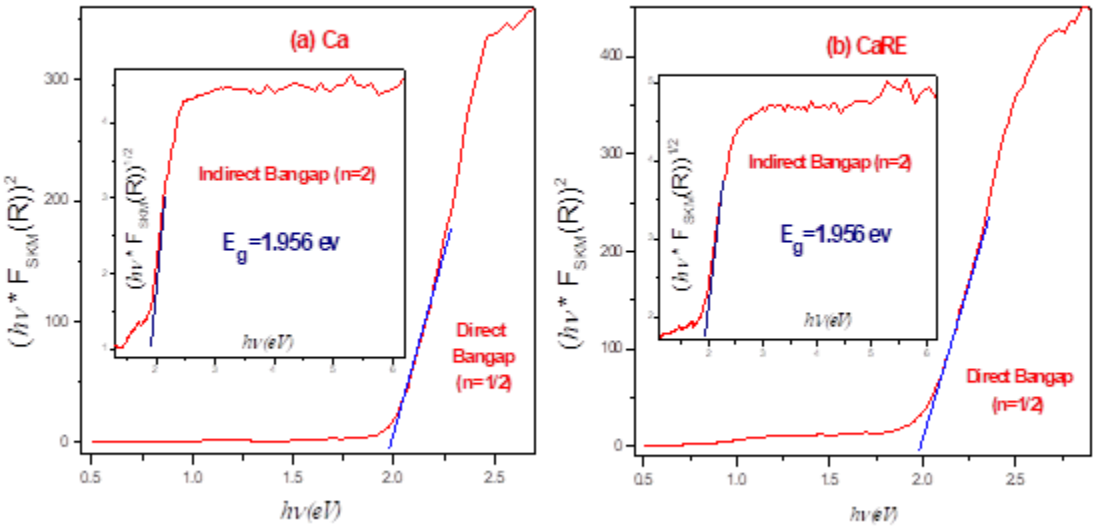

Fig 7(a-b): $(F(R_\infty)*h\nu)^2$ versus (hν) graphs for the samples.

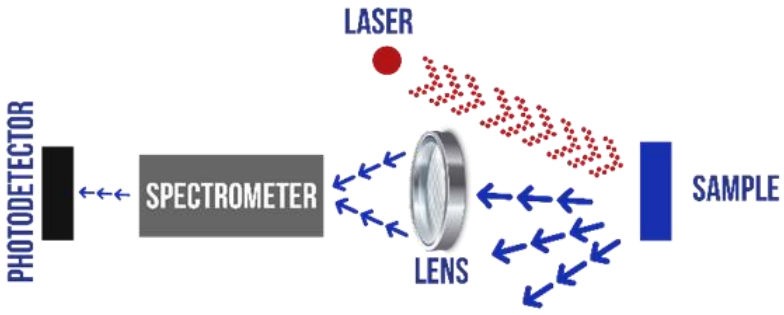

Fig 8: The concept of the Photoluminescence measurement

ISSN: 0011-9342 | Year 2021
Issue: 6 | Pages: 5143-5155

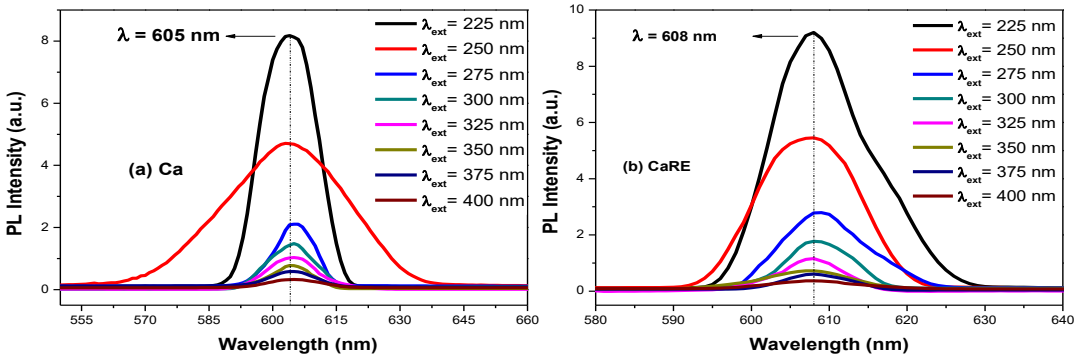

Fig 9(a-b): Photoluminescence Spectrum of (a) Ca and (b) CaRE nanoparticles.

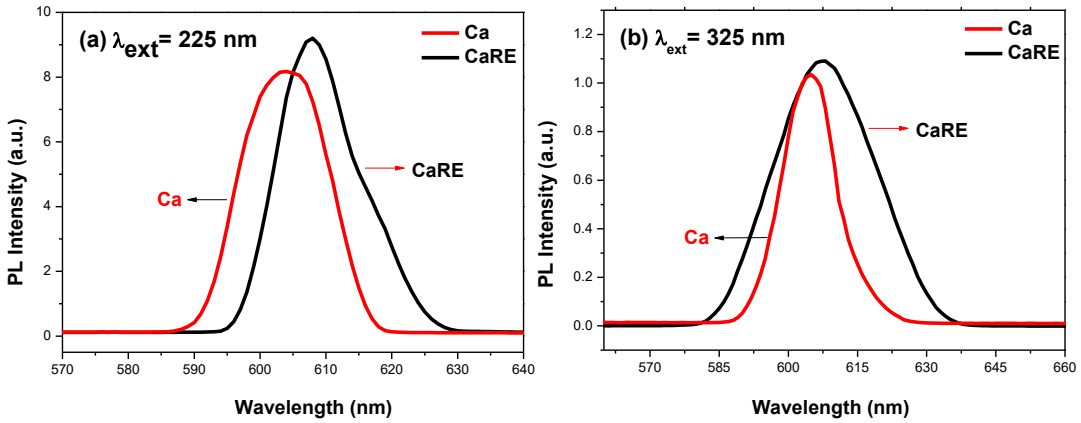

Fig 10(a-b): Photoluminescence Spectrum of Ca and CaRE obtained with excitation wavelength (a) 225 nm and (b) 325 nm.

Meanwhile, for the other excited wavelengths the band width gets smaller, with only one exception for the excited wavelength of 250 nm, where the band is much wider and varies from 560 to 640 nm. On the other hand, for the RE-doped sample, the band widths follow a similar pattern of larger width corresponding to the excited wavelength of 225 nm, but without exception. Furthermore, as displayed in Figure (10: a-b), the maximum intensity is red-shifted for the RE-doped sample. Additionally, the emitted intensity of the RE-doped sample is higher, therefore the separation of the charge carriers is relatively lower [26]

ISSN: 0011-9342 | Year 2021
Issue: 6 | Pages: 5143-5155

V. Conclusions

The proposed samples were successfully prepared in single phase as proved from the XRD matching with the parent ICDD card. Moreover, the samples grain sizes vary in the range of 25 - 65 nm, as verified by the transmission electron microscope, proving the nanometric dimension of the samples. The novel property of strong Near Infra-Red (NIR) reflectance of Calcium ferrite doped Samarium and Gadolinium sample was verified. Specifically, the diffuse reflectance spectra demonstrate the NIR reflectance improvement for the rare-earth-doped sample. Furthermore, the optical bandgap was determined for the samples with and without rare-earth doping. The allowed-direct energy gaps for the inspected samples are almost the same, about 2.0 eV. Likewise, the photoluminescence spectra reveals the same value for the energy gap. Whereas, the band gaps for the allowed-indirect transition are 1.6 and 0.9 eV for the pure and RE-doped samples, respectively. The relatively small energy gap makes the samples good candidates for water treatment by the mere application of visible light. Additionally, the wide band reflectance for the CaRE sample indicates that the system could be useful in several applications, for example, visible light transmission reduction and NIR protection.

Conflicts of Interest: "The authors declare no conflict of interest."

REFERENCES

1. H. Lv et al., "Coin-like α-Fe2O3@CoFe2O4 core-shell composites with excellent electromagnetic absorption performance," ACS Appl. Mater. Interfaces, vol. 7, no. 8, pp. 4744–4750, Mar. 2015.
2. X. Wang, X. Xu, W. Gong, Z. Feng, and R. Gong, "Electromagnetic properties of Fe-Si-Al/BaTiO3/Nd 2Fe14B particulate composites at microwave frequencies," in Journal of Applied Physics, 2014, vol. 115, no. 17.
3. Z. Yang, Z. Li, L. Yu, Y. Yang, and Z. Xu, "Achieving high performance electromagnetic wave attenuation: A rational design of silica coated mesoporous iron microcubes," J. Mater. Chem. C, vol. 2, no. 36, pp. 7583–7588, Sep. 2014.
4. J. Liu, J. Xu, R. Che, H. Chen, M. Liu, and Z. Liu, "Hierarchical Fe3O4@TiO2 yolk-shell microspheres with enhanced microwave-absorption properties," Chem. - A Eur. J., vol. 19, no. 21, pp. 6746–6752, May 2013.
5. X. J. Zhang et al., "Enhanced microwave absorption property of reduced graphene oxide (RGO)-MnFe2O4 nanocomposites and polyvinylidene fluoride," ACS Appl. Mater. Interfaces, vol. 6, no. 10, pp. 7471–7478, May 2014.
6. Y. Cui et al., "Plasmonic and Metamaterial Structures as Electromagnetic Absorbers."
7. Y. X. Yeng et al., "Enabling high-temperature nanophotonics for energy applications," Proc. Natl. Acad. Sci. U. S. A., vol. 109, no. 7, pp. 2280–2285, Feb. 2012.
8. M. A. A. Abdelkareem et al., "Vibration energy harvesting in automotive suspension system: A detailed review," Applied Energy, vol. 229. Elsevier Ltd, pp. 672–699, 01-Nov-2018.

ISSN: 0011-9342 | Year 2021
Issue: 6 | Pages: 5143-5155

9. C. Ma, J. Yan, Y. Huang, C. Wang, and G. Yang, “The optical duality of tellurium nanoparticles for broadband solar energy harvesting and efficient photothermal conversion,” Sci. Adv., vol. 4, no. 8, p. eaas9894, Aug. 2018.
10. S. Layek and H. C. Verma, “Magnetic and dielectric properties of multiferroic BiFeO3 nanoparticles synthesized by a novel citrate combustion method,” Adv. Mater. Lett., vol. 3, no. 6, pp. 533–538, Dec. 2012.
11. A. M. Fawzy, A. K. Eessaa, and Y. A. Saeid, “Energy gap variation due to al content in SmFe<inf>1−x</inf>Al<inf>x</inf>O<inf>3</inf> and its application in optics,” Micro Nano Lett., vol. 13, no. 11, 2018.
12. M. Zhang, T. An, X. Hu, C. Wang, G. Sheng, and J. Fu, “Preparation and photocatalytic properties of a nanometer ZnO-SnO 2 coupled oxide,” Appl. Catal. A Gen., vol. 260, no. 2, pp. 215–222, 2004.
13. B. M. Weckhuysen and R. A. Schoonheydt, “Recent progress in diffuse reflectance spectroscopy of supported metal oxide catalysts,” Catal. Today, vol. 49, no. 4, pp. 441–451, 1999.
14. A. A. Kokhanovsky, “Physical interpretation and accuracy of the Kubelka-Munk theory,” J. Phys. D. Appl. Phys., vol. 40, no. 7, pp. 2210–2216, Apr. 2007.
15. G. Ranga Rao and H. Ranjan Sahu, “XRD and UV-Vis diffuse reflectance analysis of CeO2-ZrO2 solid solutions synthesized by combustion method,” Proc. Indian Acad. Sci. Chem. Sci., vol. 113, no. 5–6, pp. 651–658, 2001.
16. J. Tauc, “Optical Properties of Non-Crystalline Solids,” in Optical Properties of Solids, F. Abelès, Ed. Amsterdam: North-Holland Publishing Company, 1972, pp. 277–314.
17. E. A. Davis and N. F. Mott, “Conduction in non-crystalline systems V. Conductivity, optical absorption and photoconductivity in amorphous semiconductors,” Philos. Mag., vol. 22, no. 179, pp. 903–922, 1970.
18. S. Komornicki, L. Fournès, J. C. Grenier, F. Ménil, M. Pouchard, and P. Hagenmuller, “Investigation of mixed valency ferrites La1-xCaxFeO3-y (0<x<0.50) with the perovskite structure,” Mater. Res. Bull., vol. 16, no. 8, pp. 967–973, 1981.
19. K. K. Patankar, P. D. Dombale, V. L. Mathe, S. A. Patil, and R. N. Patil, “AC conductivity and magnetoelectric effect in MnFe1.8Cr0.2O4-BaTiO3 composites,” Mater. Sci. Eng. B Solid-State Mater. Adv. Technol., vol. 87, no. 1, pp. 53–58, Oct. 2001.
20. K. W. Wagner, “Zur Theorie der unvollkommenen Dielektrika,” Ann. Phys., vol. 345, no. 5, pp. 817–855, 1913.
21. R. K. Singh et al., “Thermal, structural, magnetic and photoluminescence studies on cobalt ferrite nanoparticles obtained by citrate precursor method,” in Journal of Thermal Analysis and Calorimetry, 2012, vol. 110, no. 2, pp. 573–580.
22. B. Ghosh et al., “Origin of the Photoluminescence Quantum Yields Enhanced by Alkane-Termination of Freestanding Silicon Nanocrystals: Temperature-Dependence of Optical Properties,” Sci. Rep., vol. 6, no. 1, pp. 1–11, Nov. 2016.
23. Y. A. S. Ahmed Mohamed Fawzy, Ashraf kamal Eessaa, “Synthesis and the Study of Optical

ISSN: 0011-9342 | Year 2021
Issue: 6 | Pages: 5143-5155

Characteristics of Nano SmFe 1-x Al x O 3 by the Double Sintering Ceramic Method."
24. R. Cheng, L. Zhang, X. Fan, M. Wang, M. Li, and J. Shi, "One-step construction of FeOx modified g-C3N4 for largely enhanced visible-light photocatalytic hydrogen evolution," Carbon N. Y., vol. 101, pp. 62–70, May 2016.
25. G. Ranga Rao and H. Ranjan Sahu, "XRD and UV-Vis diffuse reflectance analysis of CeO2-ZrO2 solid solutions synthesized by combustion method," in Proceedings of the Indian Academy of Sciences: Chemical Sciences, 2001, vol. 113, no. 5–6, pp. 651–658.
26. S. Vadivel, D. Maruthamani, A. Habibi-Yangjeh, B. Paul, S. S. Dhar, and K. Selvam, "Facile synthesis of novel CaFe2O4/g-C3N4 nanocomposites for degradation of methylene blue under visible-light irradiation," J. Colloid Interface Sci., vol. 480, pp. 126–136, Oct. 2016.